Rectangular rutile TiO$_2$ nanorod arrays grown on TiO$_2$ nanotubes and enhanced visible-light photocatalytic activity

BITAO LIU[a,b], TING SUN[b], LIANGSHENG GE[b], JIAFU XU[b], HAIYAN YU[b], YA WANG[b], LIANGLIANG TIAN[a,b,*], WEI XIAO[a,b,*]
aCollege of Materials and Chemical Engineering, Chongqing University of Arts and Sciences, Chongqing, 402160, China
bDepartment of Research Center for Materials Interdisciplinary Science, Chongqing University of Arts and Sciences, Chongqing, 402160, China

TiO$_2$ nanorods (NRs) growth on the mix-phased porous TiO$_2$ nanotubes (NTs) was synthesized by an emulsion electrospinning and hydrothermal process. The as-obtained new structure of TiO$_2$ NRs/NTs was then characterized by field emission scanning electron microscopy (FESEM), transmission electron microscopy (TEM), and X-ray diffraction pattern (XRD). The photocatalytic activity was also investigated. It was found that this newly structured TiO$_2$ photocatalyst exhibited enhanced photocatalytic activity under visible light irradiation, which should ascribe to its efficient electron-hole separation in this new structure.

1. Introduction

Owing to its low cost, high chemical inertness, and environmental applications (high catalytic activity for the removal of pollutants in water and air), TiO$_2$ has been intensively investigated in photocatalysis [1, 2]. The two principal catalytic phases of TiO$_2$, anatase and rutile, have numerous structural and functional differences. Commercially available anatase is typically less than 50 nm in size. These particles have a band gap of 3.2 eV, corresponding to a UV wavelength of 385 nm. The anatase exhibits lower rates of recombination in comparison to rutile due to its 10-fold greater rate of hole trapping [3]. In contrast, though some exceptions exist, the thermodynamically stable rutile phase generally exists as particles larger than 200 nm [3]. Rutile has a smaller band gap of 3.0 eV with excitation wavelengths that extend into the visible at 420 nm; furthermore, it should be more populated after allowing time for electron transfer [3]. It is reported that mixed phase TiO$_2$ show excellent charge separation ability, such as commercial powders Degussa P25 [3, 4]. However, nano sized TiO$_2$ is difficult to recycle from aqueous solution after photocatalytic reactions and will cause secondary pollution [5]. To solve this problem, large scaled mesoporous spheres [6], thin films [7] and one-dimensional [4, 8] have been investigated by many research groups since they have large surface area and better electron separation ability.

In this work, a newly structured TiO$_2$ synthesized by an emulsion electrospinning and hydrothermal process, where one-dimensional highly porous TiO$_2$ NTs were used as an electron separation for TiO$_2$ NRs. The as-obtained newly structured TiO$_2$ nanotubes also were investigated for their catalytic performances against the degradation of Methyl Orange (MO). The study revealed that these newly structured TiO$_2$ nanotubes structure appear to be promising photocatalysts.

2. Experimental

A schematic illustration of the growth of NRs on the TiO$_2$ NT is shown in Fig. 1. The highly porous TiO$_2$ NTs were prepared by an emulsion electrospinning process as depicted in our former work [4], and the TiO$_2$ NR/NTs were then synthesized by a simple hydrothermal reaction. In a typical procedure, 1 ml tetrabutyl titanate was dissolved in 30 ml 9 M HCl solution, then 0.1g TiO$_2$ NTs were added, and finally followed by 10 minutes of ultrasonication. Subsequently, the mixture was transferred to a 50 mL Teflon-lined autoclave maintained at 180 °C for 1 to 10 h. Finally, the product was washed and dried.

Fig. 1. Schematic representation of TiO$_2$ NR/NT.

The morphologies were observed by FESEM (Hitachi, S-4800), and TEM (FEI Tecnai F30). Crystal phase of the obtained materials were determined by powder XRD (Rigaku D/MAX-2400). In the photodegradation process, 20 mg of the catalyst was suspended in 160 mL of 10 ppm MO dyes solution, after stirred in dark for 30 min, the solution was then exposed to the visible light irradiation produced by a 500W Xe arc lamp equipped with a band-pass light filter (>400 nm). Varian UV-Vis spectrophotometer (Cary-50, Varian Co.) were used.

3. Results and discussions

Fig. 2a and b showed the SEM and TEM images of TiO$_2$ NTs. They clearly indicated that these nanotubes have a tubular structure with outer diameters of *ca.* 200 nm, wall thickness of 40–60 nm, and numerous pores on the wall. These pores with an approximate diameter of 10–20 nm were distributed evenly due to the improved emulsion electrospinning process [4]. Fig. 1c showed a typical SEM image of TiO$_2$ NR/NT after hydrothermal reaction at 180 °C for 5 h. As shown, the entire outer and inner surfaces of the NTs were covered uniformly by TiO$_2$ NRs that were tetragonal in shape with square top facets. The diameter and length of the nanorods were found to be ~10 nm and ~150 nm, respectively. The typical TEM/HRTEM images were shown in Fig. 2d-f. As shown, the nanorods were evenly distributed on the mesoporous nanotubes. The phase and crystal structure of the TiO$_2$ NRs were confirmed by the lattice image in Fig. 1f. The distances between lattice fringes, 0.32 and 0.29 nm, could be assigned to (110) and (001) of the rutile TiO$_2$ phase, respectively, suggesting that the TiO$_2$ NRs grew along the [001] axis. The corresponding selected-area's electron diffraction (SAED) pattern (Fig. 1f) displayed the single-crystalline nature and should index to the pure rutile TiO$_2$ phase.
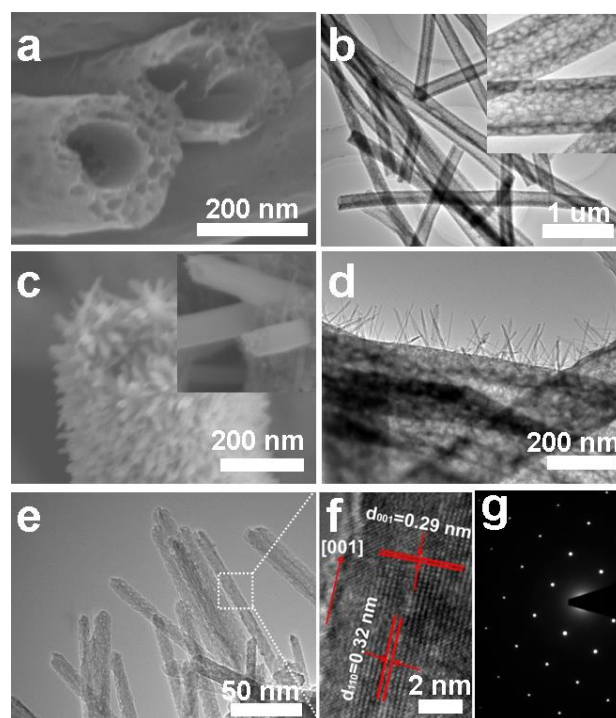
Fig. 2. SEM and TEM images of TiO$_2$ NT (a, b); SEM, TEM, HRTEM image and SAED pattern of TiO$_2$ NR (c, d, e, f, g).

Detailed growth process with different reaction times was in shown Fig. 3. For the 1h sample, the NRs on the NT were sparely grown and the length was about 100 nm. As time increased, the NRs became dense, and the length increased to 130 nm and 500 nm for the 5 and 10 h samples, respectively. Nevertheless, the diameter of these NRs still remained the same size of about ~10 nm. The increased length and unchanged diameter resulted in a larger surface area.
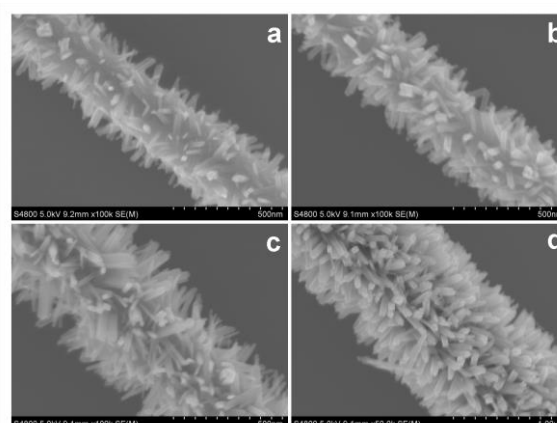
Fig. 3. SEM images of series TiO$_2$ NR/NT with different hydrothermal reaction times (a: 1h; b: 3h; c: 5h; d: 10h).

XRD patterns of the as-prepared series samples were shown in Fig. 4. All the samples were consisted with mixed crystalline phases of anatase and rutile. As reaction time increased, the diffraction of rutile (110) facets remarkably increased, which demonstrated that the TiO$_2$ NRs grew along the [001] axis. According to the empirical relationship by Deperoet al, [9] the ratio between these phases determined from the XRD spectra can be estimated by the following equation:

$$R(T) = 0.679 \frac{I_R}{I_R + I_A} + 0.312 \left(\frac{I_R}{I_R + I_A} \right)^2 \qquad (1)$$

where R(T) is the percentage content of rutile, I$_A$ is the intensity of the main anatase reflection, and I$_R$ is the intensity of the main rutile reflection [9]. The ratio of the porous TiO$_2$ NTs of rutile phase to anatase phase was 22:78, and for the TiO$_2$ NR/NT samples, this ratio increased to 35:65, 44:56, 63:37 and 83:17, respectively.
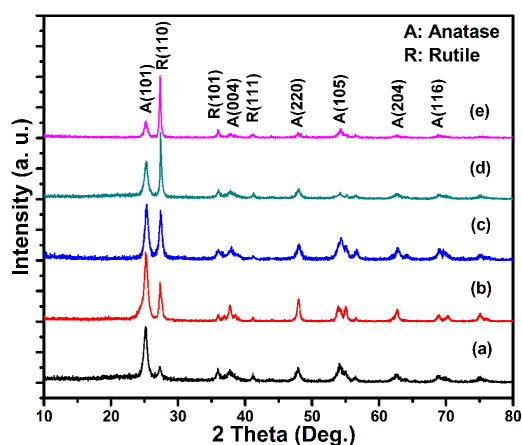
Fig. 4. XRD patterns of TiO$_2$ NT (a) and TiO$_2$ NR arrays growth of on TiO$_2$ NT with different hydrothermal reaction times (b: 1h; c: 3h; d: 5h; e: 10h).

For a better understanding of the energy levels in the band-gap of semiconductor materials, PL spectral as exhibited in Fig. 5 were introduced which would influence the charge transport and recombination properties in photocatalysis [10]. The PL bands can be fitted into three Gaussian peaks with wavelengths of 422-425 nm, 521-525 nm and 627-629 nm and 832-834 nm. Generally, these spectra can interpreted as the emission from three physical origins: self-trapped excitons [11, 12], oxygen vacancies (OVs) [13, 14] and surface states [15]. As reported in many work and our previous work [4, 12-17], the peak position of the 422-425 nm band should assigned to self-trapped excitons (STE) localized on TiO$_6$ octahedra [12], the 521-525 nm (0.82-0.84eV) bands should attribute to OVs located at the surface of the TiO$_2$ nanoparticles (SOVs) [14, 15], and the PL bands at 627-629 nm should

assign to emission from oxygen vacancies [16, 17]. Meanwhile, the PL band at ~832 nm can ascribe to the intrinsic properties of rutile phase TiO$_2$ [18, 19]. However, the PL intensity of the rutile phase TiO$_2$ was much lower than the anatase phase.
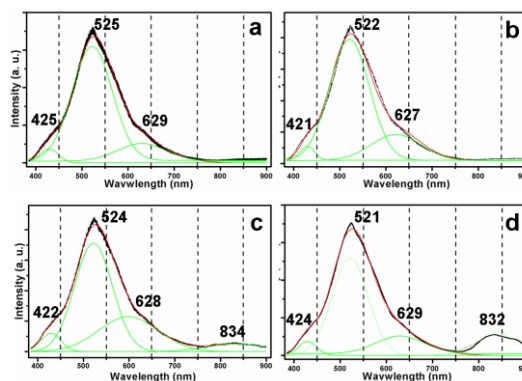
Fig. 5. PL spectra of TiO$_2$ NR arrays growth of on TiO$_2$ NT with different hydrothermal reaction times (a: 1h; b: 3h; c: 5h; d: 10h).

This result is interesting, because it has been established that rutile exhibits high rates of recombination in comparison to anatase, so, there would be easier to observe a PL band of rutile phase [20, 21]. Due to this special structure, we deduced that the excited excitons in rutile phase would trapped by the SOVs in anatase phase. This hypothesis can be proved by a direct measure of the change in the PL intensity. As can be seen, only the rutile phase ratio is high as 63% (Fig. 5c, 5 h hydrothermal sample), the rutile trapping sites can be observed, and the intensity is still lower than the anatase trapping sites and surface trapping sites (OVs and SOVs in anatase phase). This confirms the transfer of rutile electrons to anatase. The electron-transfer reaction has an estimated activation barrier of less than 8.3×10^{-4} eV based on the measured rate of transfer [22]. Lower activation energy of electron transfer should be possible. However, too much rutile phase also would result a higher recombination in the rutile phase as shown in Fig. 5d, which would not benefit to the photocatlyst process.

Fig. 6a showed time profile of MO absorbance spectra observed during the incubation with TiO$_2$ NR/NT (5 h) under visible light irradiation. The absorption peaks at 465 nm correspond to dimers and monomers of MO. As shown, the spectra intensity showed a gradual decrease with the increase of irradiation time. For the evaluation of degradation kinetics of MO, we measured the change of main absorption peak at 465 nm as shown in Fig. 6b. When comparing the photocatalytic activities among these samples, all the TiO$_2$ NR/NT samples showed a higher activity for MO degradation than TiO$_2$ NT, especially in the dark absorption. The 5 h sample exhibited the highest

activity with a degradation rate of 68.9% while the TiO_2 NTs' degradation rate was only 49.5%. A proposed schematic illustration could be shown in the inset of Fig. 6. The presence of rutile NRs would create a structure where under visible illumination, rapid electron transfer would take place from rutile to lower energy anatase lattice trapping sites that then lead to a more stable charge separation [3, 23]. The photo-generated electron transfer from rutile to anatase lattice trapping sites allowed holes, which would have been annihilated due to recombination, to reach the surface. Subsequent electron-transfer moves the electron from anatase trapping sites to surface trapping sites, further separating the electron/hole pair [3]. By competing with recombination, the stabilization of charge separation activated the catalyst and the rutile-originating hole could then participate in oxidative chemistry [3]. The one-dimensional structure could also provide a dual-channel for the transportation of electrons separation [24]. Additionally, these NRs should not be too long, for fear of being disadvantageous for the electron separation, and would lead a lower photocatalytic activity as showed in the 10 h sample. This should ascribe to the limited charge transport distance [25].
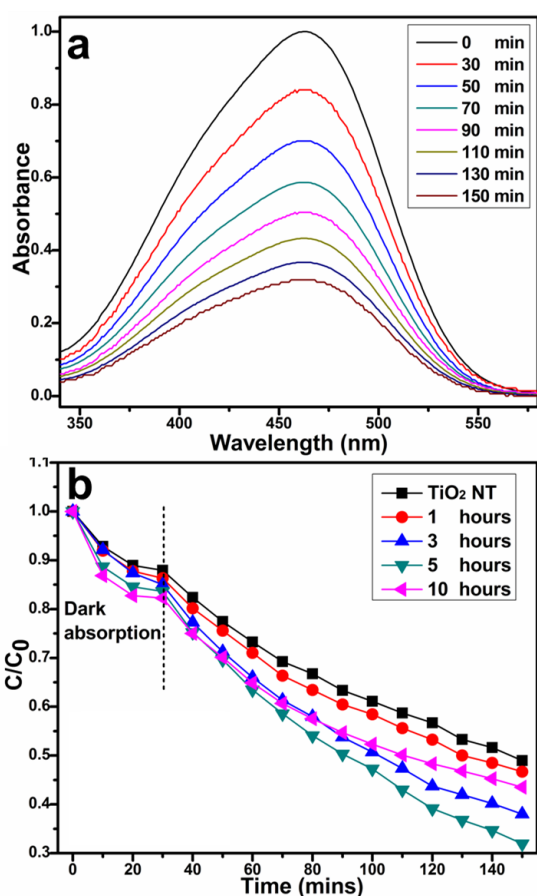
Thus, a proposed schematic illustration was shown as Fig. 7. The presence of rutile phase nanorods would create a structure where rapid electron transfer from nanorodes to lower energy anatase nanotube under visible illumination, which leads to a stable charge separation [3, 23]. By competing with recombination of the electron/hole pairs, the charge separation would activate the catalyst and the rutile-originating hole would participate in oxidative chemistry [3]. Obviously, a higher catalytic activity in this new structure should ascribed to the more efficient electron transfer from rutile to the lower trapping sites in anatase, and too much more rutile phase also would leading a higher recombination.
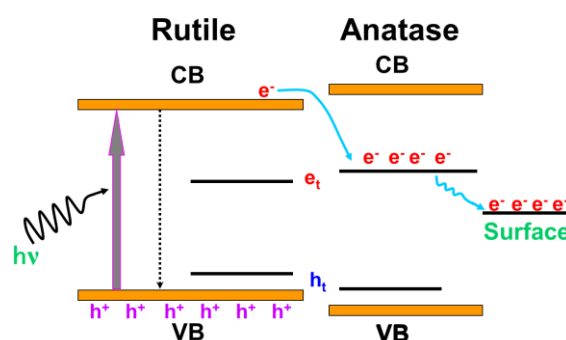
Fig. 7. A proposed schematic illustrations showing the reaction mechanism   for photocatalytic degradation of organic pollutants under visible light irradiation.

4. Conclusion

Newly structured TiO_2 NR/NTs were synthesized by an emulsion electrospinning and hydrothermal process. The photocatalytic activity of MO was also investigated. It was found that this newly structured TiO_2 photocatalyst exhibited enhanced catalytic activity under visible light irradiation than the original TiO_2 NTs. This could be ascribed to its efficient electron-hole separation in this new structure. The 5h TiO_2 NR/NT sample exhibited best photocatalytic activity with degradation rate of 68.9% after 150 min. This newly obtained structure of TiO_2 NR/NT is now a member in the family of photocatalytic materials and may serve useful purposes in other applications such as hydrogen preparation, lithium ion batteries and so on.

Acknowledgements

Fig. 6. Absorbance spectra of TiO₂ NR/NT (5h) under visible light   irradiation (a) and Photo-degradation of MO under visible light by different samples (b).

Reference

[1] J. Du, X. Y. Lai, N. L. Yang, J. Zhai, D. F. Kisailus, B. Su, Wang D, L. Jiang. ACS Nano, **5**, 590 (2011).

[2] B. T. Liu, Y. J. Huang, Y. Wen, L. Du, W. Zeng, Y. R. Shi, F. Zhang, G. Zhu, X. Xu, Y. H. Wang. J. Mater. Chem. **22**, 7484 (2012).

[3] D. C. Hurum, A. G. Agrios, K. A. Gray, T. Rajh, M. C. Thurnauer, J. Phys. Chem. B, **107**, 4545 (2003).

[4] B. T. Liu, L. L. Peng. J Alloys Compd, **571**, 145 (2013).

[5] X. X. Yu, J. Yu, B. Cheng. M. Jaroniec. J Phys Chem C, **113**, 17527 (2009).

[6] D. Chen, F. Huang, Y. B. Cheng, A. Rachel. Advanced Materials, **21**, 2206 (2009).

[7] B. Liu, E. S. Aydil. Chem. Commun. **47**, 9507 (2011).

[8] B. A. Lu, C. Q. Zhu, Z. Zhang, W. Lan, E. Q. Xie. J. Mater. Chem. **22**, 1375 (2012).

[9] L. E. Depero, L. Sangaletti, E. B. B. Allieri, R. Salari, M. Zocchi, C. Casale, M. Notaro. J. Mater. Res. **13**, 1644 (2000).

[10] C. Pan, J. Xu, Y. Wang, D. Li, Y. Zhu, Adv. Funct. Mater., **22**, 1518 (2012).

[11] H. Tang, H. Berger, P. E. Schmid, F. Lévy, G. Burri, Solid State Commun. **87**, 847 (1993).

[12] Y. Lei, L. D. Zhang, G. W. Meng, G. H. Li, X. Y. Zhang, C. H. Liang, W. Chen, S. X. Wang, Appl. Phys. Lett., **78**, 1125 (2001).

[13] N. Serpone, D. Lawless, R. Khairutdinov, J. Phys. Chem., **99**, 16646 (1995).

[14] L. V. Saraf, S. I. Patil, S. B. Ogale, S. R. Sainkar, S. T. Kshirsager, Int. J. Mod. Phys. B, **12**, 2635 (1998).

[15] L. Forss, M. Schubnell, Appl. Phys. B, **56**, 363 (1993).

[16] D. C. Cronemeyer, Phys. Rev. 113 (1959) 1222.

[17] X. Li, C. Gao, J. Wang B., Lu, W. Chen, J. Song, S. Zhang, Z. Zhang, X. Pan, E. Xie, Journal of Power Sources, **214**, 244 (2012).

[18] F. Montoncello, M. C. Carotta, B. Cavicchi, M. Ferroni, A. Giberti, V. Guidi, C. Malagu, G. Martinelli, F. Meinardi, J. Appl. Phys. **94**, 1501 (2003).

[19] A. Amtout, R. Leonelli, Phys. Rev. B, **51**, 6842 (1995).

[20] G. Riegel, J. R. Bolton, J. Phys. Chem., **99**, 4215 (1995).

[21] A. Sclafani, J. M. Herrmann, J. Phys. Chem. **100**, 13655 (1996).

[22] P. W. Atkins, Physical Chemistry, 5th ed.; W. H. Freeman and Company: New York, 1994, 877.

[23] R. L. Penn, J. F. Banfield, Am. Mineral. **84**, 871 (1999).

[24] J. Wang, Z. Q. Lin. Chem. Mater. **20**, 1257 (2008).

[25] X. Zhang, V. Thavasi, S. G. Mhaisalkar, S. Ramakrishn Nanoscale. **4**, 1707 (2012).

*Corresponding author: tianll07@163.com